



This is a repository copy of *Molecular ejection transition in liquid crystal columns self-assembled from wedge-shaped minidendrons*.

White Rose Research Online URL for this paper:
<https://eprints.whiterose.ac.uk/139364/>

Version: Accepted Version

Article:

Fall, W.S. orcid.org/0000-0001-6778-1348, Yen, M.-H., Zeng, X. orcid.org/0000-0003-4896-8080 et al. (4 more authors) (2019) Molecular ejection transition in liquid crystal columns self-assembled from wedge-shaped minidendrons. *Soft Matter*, 15 (1). pp. 22-29. ISSN 1744-683X

<https://doi.org/10.1039/c8sm01851k>

© The Royal Society of Chemistry 2018. This is an author produced version of a paper subsequently published in *Soft Matter*. Uploaded in accordance with the publisher's self-archiving policy.

Reuse

Items deposited in White Rose Research Online are protected by copyright, with all rights reserved unless indicated otherwise. They may be downloaded and/or printed for private study, or other acts as permitted by national copyright laws. The publisher or other rights holders may allow further reproduction and re-use of the full text version. This is indicated by the licence information on the White Rose Research Online record for the item.

Takedown

If you consider content in White Rose Research Online to be in breach of UK law, please notify us by emailing eprints@whiterose.ac.uk including the URL of the record and the reason for the withdrawal request.



eprints@whiterose.ac.uk
<https://eprints.whiterose.ac.uk/>

Cite this: DOI: 10.1039/xxxxxxxxxx

Molecular Ejection Transition in Liquid Crystal Columns Self-Assembled from Wedge-Shaped Minidendrons[†]

 William S. Fall,^{a,b} Ming-Huei Yen,^c Xiangbing Zeng,^c Liliana Cseh,^d Yongsong Liu,^a Gillian A. Gehring,^{*b} and Goran Ungar^{*a,c}

Received Date

Accepted Date

DOI: 10.1039/xxxxxxxxxx

www.rsc.org/journalname

Fan-shaped molecules with aromatic head-groups and two or more flexible pendant chains often self-assemble into columns that form columnar liquid crystals by packing on a 2d lattice. Such dendrons or minidendrons are essential building blocks in a large number of synthetic self-assembled systems and organic device materials. Here we report a new type of phase transition that occurs between two hexagonal columnar phases, Col_h1 and Col_h2, of Na-salt of 3,4,5-tris-dodecyloxy benzoic acid. Interestingly the transition does not change the symmetry, which is *p6mm* in both phases, but on heating it involves a quantised drop in the number of molecules $\langle n \rangle$ in the cross-section of a column. The drop is from 4 to 3.5, with a further continuous decrease toward $\langle n \rangle = 3$ as temperature increases further above T_c . The finding is based on evidence from X-ray diffraction. Using a transfer matrix formulation for the interactions within a column, with small additional mean field terms, we describe quantitatively the observed changes in terms of intermolecular forces responsible for the formation of supramolecular columns. The driving force behind temperature-induced molecular ejection from the columns is the increase in conformational disorder and the consequent lateral expansion of the alkyl chains. The asymmetry of the transition is due to the local order between 4-molecule discs giving extra stability to purely $\langle n \rangle = 4$ columns.

Introduction

Taper-shaped molecules such as the tree-like “dendrons” have been shown to exhibit rich phase behavior by self-assembly into supramolecular sheets, columns or spheres. Dendrons displaying such liquid crystal (LC) phases usually comprise an aromatic core with flexible chains at the periphery^{1–4}. In many fan-shaped molecules the 2d-ordered columnar phase that appears at lower temperatures transforms on heating to one or a series of 3d spherical micellar phases. These have their counterparts in metals and are either cubic such as *Pm* $\bar{3}$ *n* (A15)⁵ and body-centered cubic (BCC)⁶, or tetragonal (α -phase)⁷ or even quasicrystalline^{8,9}. Interestingly, all phases observed so far in

these series of compounds can be seen in the simplest of them, known as ‘minidendrons’^{10–12} (see e.g. Figure 1a). Taper-shaped mesogens, including minidendrons, are some of the most fundamental and widespread building blocks in supramolecular chemistry¹³. They have been attached to moieties such as organic semiconductors^{14,15}, ionic conductors^{16–20}, crown ether selective chelators^{21–23}, donor-acceptor complexes and polymers^{24,25}, peptides²⁶, nanoparticles^{27,28}, quantum dots²⁹ etc. In this way “dendronized” functional materials may be created, useful in a variety of applications³⁰.

Beside displaying an impressive array of complex 2D and 3D nanostructures, wedge-shaped and other “unusual” mesogens undergo numerous phase transitions. However studies giving a theoretical basis of such phenomena are surprisingly rare in such systems^{31,32}. In more traditional LC’s, i.e. nematic and smectic, structures and transitions have been described theoretically in a number of cases by “borrowing” models from other areas of condensed matter and understood in the framework of the same physical principles. Well known examples include the nematic to smectic-A transition³³, the twist-grain-boundary (TGB) smectic phase³⁴ and the hexatic phases³⁵, the latter being real-life examples of the Kosterlitz-Thouless theory of 2d melting³⁶. The

^a Department of Physics, Zhejiang Sci-Tech University, Xiasha College Park, Hangzhou 310018, China

^b Department of Physics and Astronomy, University of Sheffield, Sheffield S3 7RH, U.K.

^c Department of Materials Science and Engineering, University of Sheffield, Sheffield S1 3JD, U.K.

^d Institute of Chemistry Timisoara of Romanian Academy, Timisoara - 300223, Romania

[†] Electronic Supplementary Information (ESI) available: [details of any supplementary information available should be included here]. See DOI: 10.1039/cXsm00000x/

present work describes an unusual transition, one that happens within the same $p6mm$ hexagonal columnar phase. We show that the ordering of a LC column may be described using the formalism of a magnetic spin chain. Interestingly an approach linking magnetism and another type of complex soft self-assembly, i.e. multicolour tiling in a honeycomb LC^{37,38}, is to our knowledge so far the only other example in complex LC's.

In the hexagonal columnar phase (Col_h) wedge shaped molecules assemble to form supramolecular discs which in turn stack to form columns³⁹. With increasing temperature these columns show typically a continuous lateral shrinkage while maintaining positive bulk expansion^{10,11,40}. This has been attributed to continuous shedding of dendrons along the supramolecular column. An optimal average number of molecules per disc, $\langle n \rangle$, exists at a given temperature such that the overall system free energy is minimized. With increasing temperature, the dendrons expand sideways due to the increased entropy of the terminal chains, resulting in a decreasing optimal $\langle n \rangle$, and shedding of surplus dendrons. Similar behavior is observed in the cubic phases where spherical micelles shed their conically shaped dendrons continuously, thus shrinking with increasing temperature¹⁰, in some cases down to half their size at low temperatures⁴¹.

All cases so far show continuous thermal shrinkage. Herein we report a special case where the lateral shrinkage of the columns is discontinuous, involving a new type of first-order transition between two columnar LC phases of the same hexagonal symmetry but with a quantised change in the average number of molecules in a supramolecular disc. We present experimental evidence and a quantitative statistical model of this unique LC phenomenon.

Experimental Results

X-ray Diffraction and Calorimetry

The compounds used in this study are Na and Li salts of 3,4,5-trisdodecyl benzoic acid. They are labeled 12Na and 12Li and are shown in Figure 1a, together with their calorimetry (DSC) scans. Powder small-angle X-ray scattering (SAXS) curves recorded on heating are shown in Figure 1b. While 12Li shows only two LC phases, a hexagonal columnar (Col_h) and a body centered cubic (BCC), 12Na displays a sequence of four LC phases. Crystals melt into a centered rectangular columnar phase (Col_r), symmetry $c2mm$, which gradually transforms into Col_h , plane group $p6mm$, around 82°C (see Figure 2a). Above 120-125°C the columnar transforms into the cubic A15 phase, symmetry $Pm\bar{3}n$. At the same time crystalline compound 12Li melts directly into the Col_h phase which subsequently transforms into BCC.

Whilst in most other salts the hexagonal lattice parameter, a_h , i.e. the distance between column axes, decreases continuously with increasing T ^{10,11}, both 12Li and 12Na are exceptional. In 12Li a_h is virtually independent of temperature⁴² - see Figure 2. Even more interestingly, in 12Na a clear first order transition is observed between two columnar hexagonal phases, labeled Col_h1 and Col_h2 , as shown in Figures 1 and 2.

Changes in lattice parameters with temperature for 12Na and 12Li are given in Figure 2a. The first hexagonal phase of 12Na

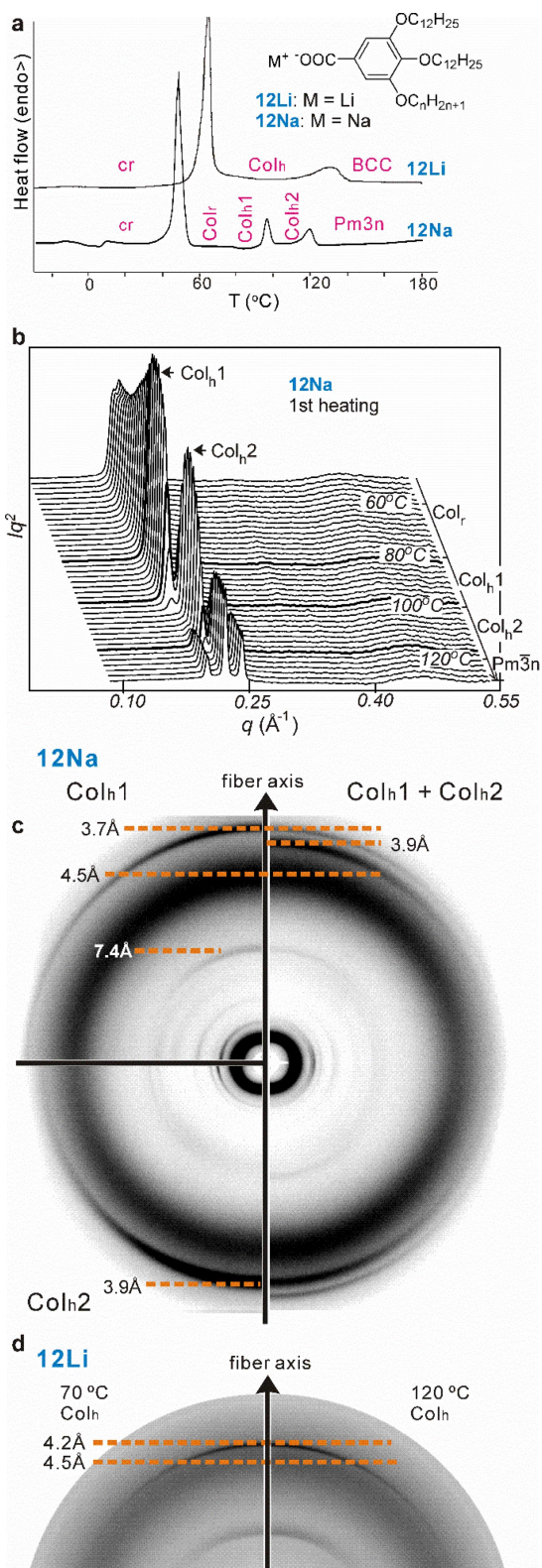


Fig. 1 (a) The compounds and their first DSC heating scans (5 K/min). Phase abbreviations: cr = crystal; Col_r = rectangular columnar phase ($c2mm$ symmetry); Col_h , Col_h1 , Col_h2 = hexagonal columnar phases ($p6mm$); BCC and $Pm\bar{3}n$ = body-centered and A15 cubic phases, respectively. (b) Temperature evolution of SAXS curve of 12Na on 1st heating at 5 K/min. (c) WAXS patterns of an extruded 12Na fiber in the Col_h1 phase at 85°C (top left), Col_h2 phase at 105°C (bottom left) and the mixture of phases ($\text{Col}_h1 + \text{Col}_h2$) at 95°C (right). (d) Part of WAXS pattern of an extruded fiber of 12Li in the Col_h phase at 70°C (left) and 120°C (right).

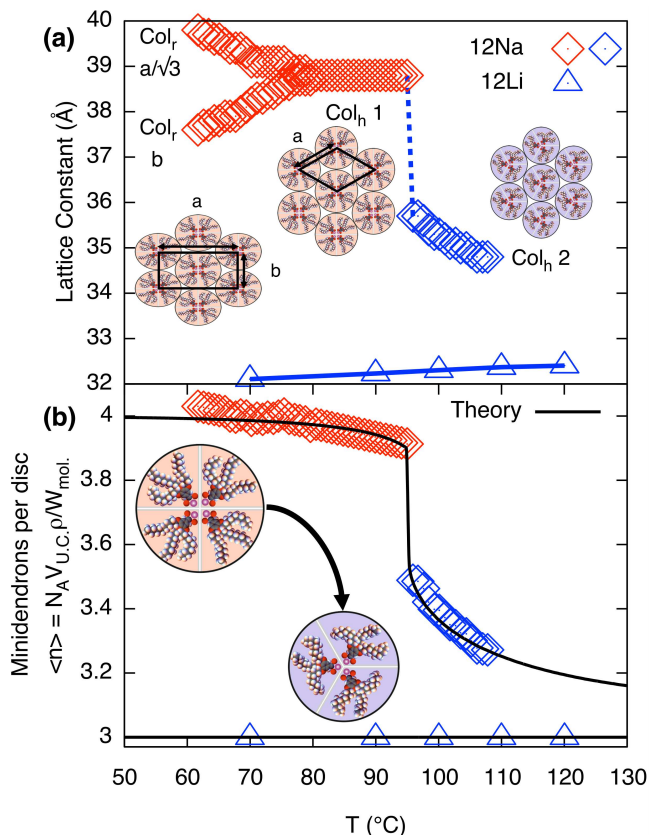


Fig. 2 (a) Intercolumnar distance in compounds 12Na and 12Li on heating, along with schematic drawings of each structure: Col_r, Col_{h1} and Col_{h2}. (b) Calculated number of minidendrons per supramolecular disc, $\langle n \rangle$, for both compounds, along with the best-fit curve from model for 12Na. Fitting parameters are discussed in the subsequent section.

(Col_{h1}) forms at around 82 °C at the convergence of b and $a/\sqrt{3}$ of the Col_r phase. In the Col_{h1} phase the intercolumnar distance a_h remains constant at 39 Å, and at about 95 °C it suddenly decreases by approximately 3 Å to 36 Å, signifying the transition to the Col_{h2} phase. After that in the Col_{h2} phase a_h decreases gradually with increasing temperature. The transition is reversible, albeit with a considerable hysteresis.

Determining the Number of Minidendrons $\langle n \rangle$

To determine the average number of molecules $\langle n \rangle$ in a supramolecular disc, or stratum of a column we need, beside the cross-section area of the column, also the height of the stratum c and the density ρ . While there is no true 3d long-range order, the wide-angle X-ray scattering (WAXS) pattern of a partially oriented extruded fiber of 12Na shows a relatively sharp meridional arc corresponding to a spacing of 3.7 Å in Col_{h1} and 3.9 Å in Col_{h2} phase (Figure 1c). These correspond to the $\pi - \pi$ stacking distance of benzene rings along the column axis and are taken as c values. The density was measured at room temperature^{10,11} and then corrected, factoring in thermal expansion (see S1[†] and Table S3). $\langle n \rangle$, thus obtained, is plotted against temperature in Figure 2b. In the Col_{h1} phase of 12Na $\langle n \rangle$ is nearly constant at 4 molecules per stratum, dropping abruptly to 3.5 at the Col_{h1}-

Col_{h2} transition and further decreasing continuously toward 3 as T is increased further. In 12Li, on the other hand, $\langle n \rangle$ is constant at 3 within the T -range of stability of the Col_{h1} phase (Figures 2 and S1[†]).

Theory

Outline

Figure 3a shows a simplified schematic of the proposed statistical model of a column consisting of interacting supramolecular discs. Each disc may contain either 3 or 4 minidendrons which are held together by an attractive energy U_n (n is the number of minidendrons in each disc), assumed to be dominated by Coulomb interactions at the center of the disc. There are also temperature dependent free energy terms of the end chains $F_n(T)$, mainly entropic due to confinement of the molecule in a slice (1/3 or 1/4) of the disc. Interaction energy J_{mn} between two neighboring discs in a column is also included, and again considered to be dominated by Coulomb interactions. The model Hamiltonian \mathcal{H} describing a single column, in Equation 1, is constructed in terms of these interaction energies and the projection operators, $P_i^{(3)}$ and $P_i^{(4)}$ which correspond to an arbitrary disc, i , containing 3 or 4 minidendrons respectively ($P_i^{(3)} + P_i^{(4)} = 1$).

$$\begin{aligned} \mathcal{H} = & \sum_i (U_4 + F_4(T)) P_i^{(4)} + \sum_i (U_3 + F_3(T)) P_i^{(3)} \\ & + \sum_i J_{44} P_i^{(4)} P_{i+1}^{(4)} + \sum_i J_{33} P_i^{(3)} P_{i+1}^{(3)} \\ & + \sum_i J_{43} (P_i^{(4)} P_{i+1}^{(3)} + P_i^{(3)} P_{i+1}^{(4)}) \end{aligned} \quad (1)$$

Equilibrium properties of a single column are calculated from Equation 1, assuming that molecules are in a heatbath and a reservoir of free molecules. Weak inter-columnar interactions are included later to take into account long-ranged interactions both along and across columns.

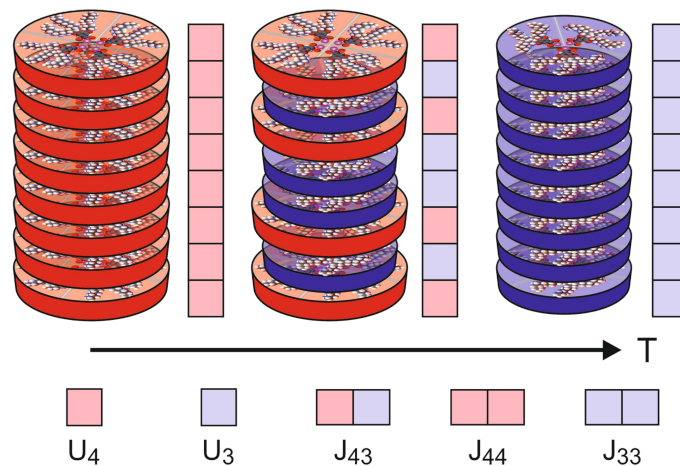


Fig. 3 Model of interacting supramolecular discs of 3 or 4 minidendrons per disc showing the pure (4), mixed (43) and pure (3) phases with increasing temperature. The intra-disc interactions U_n , and inter-disc interactions J_{mn} are also indicated.

Calculating the Chain Free Energy $F_n(T)$

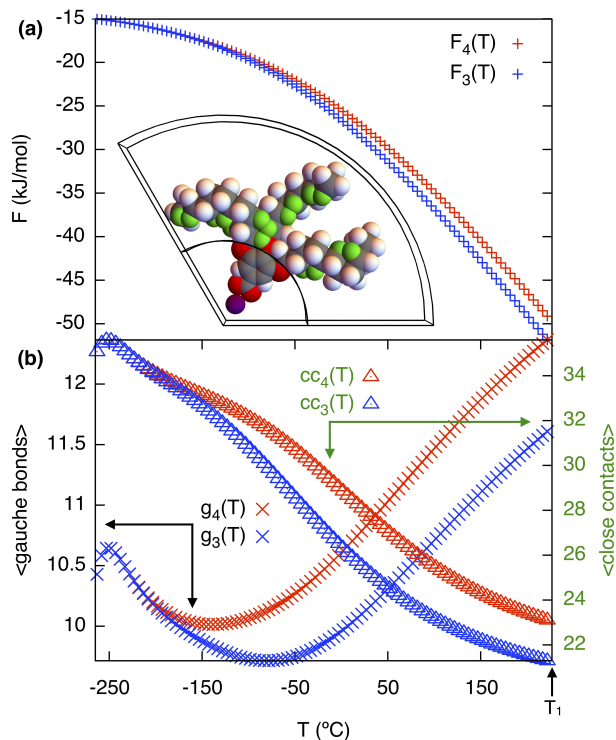


Fig. 4 (a) Chain free energy curves with a confined minidendron in a 120° segment shown in the inset, close contacts are shown in green. (b) gauche bonds g_n and close contacts cc_n vs. temperature in respective geometries. 90° (red) and 120° (blue) from the simulation with $\eta = 498\text{K}$, $\gamma = 0.4$ as defined in Equation 3.

Calculating the free energy of the three end chains $F_n(T)$ for a single minidendron presents an interesting problem since there are interactions with other molecules both within and between the supramolecular columns. Two important factors govern the shapes adopted by the chains at a given temperature; these are the number of gauche defects n_g and the extent of crystallisation with surrounding monomers. To simulate this effect, the minidendrons were confined within a segment with vertex angle θ and thickness d where the chains are restricted to only those conformations which contain discrete trans (t) or gauche (g) bonds, according to the Rotational Isomeric State model⁴³ - see Figure 4(a). The diamond lattice is therefore chosen as a suitable lattice upon which the end chains may arrange themselves. The [111] direction of the lattice is oriented along the axis of the segment, to ensure a symmetric distribution. The core boundary radius, R , is fixed such that volume is kept constant hence $R_{90} = \sqrt{\frac{4}{3}}R_{120}$, where $R_{90} = 10\text{\AA}$. For three free chains of length l in unrestricted space the number of possible conformations N is described by Equation 2.

$$N = \left(4 \cdot (3)^{(l-1)}\right)^3 \quad (2)$$

This is of the order 10^{17} for $l = 12$ but for self avoiding chains in confined space this number falls dramatically, in our case down to 10^7 . The simulations have been run for vertex angles $\theta = 90^\circ$

and 120° , to approximate the confinement of 4 or 3 molecules per disc respectively, at a thickness $d = 3.6\text{\AA}$, the closest allowed by the experimental thickness on a diamond lattice. It should be noted that the conformers are self avoiding such that no two H atoms may come closer than the first nearest neighbour distance. Successive gg' bonds are disallowed in the simulation to avoid H-H conflicts from 5th nearest neighbour monomer units, otherwise known as "pentane interference". All possible conformations are enumerated and the ensemble is then weighted according to Equation 3.

$$E_i = \eta(n_g - \gamma n_{cc}) \quad (3)$$

Here η is the energy cost of introducing a gauche defect, n_{cc} is the number of close contacts between first nearest neighboring H atoms and γ represents the energy drop of crystallisation and allows for freezing. In this case η is taken to be 4141 (J/mol) with and the expected increase in n_g and decrease in n_{cc} with increasing temperature was found for $\gamma = 0.4$, see Figure 4(b). The partition function can then be written as Equation 4 and the free energy $F_n(T)$ calculated.

$$\mathcal{Z} = \sum_i e^{-\beta(n_g - \gamma n_{cc})} \quad F_n(T) = -k_B T \log \mathcal{Z} \quad (4)$$

The generated free energy curves are shown in Figure 4. Both geometries appear identical at low temperature and gradually diverge as temperature is increased. Hence for the chains alone a mixed (43) phase is preferred at low temperature with an increasing preference for (3) at higher temperatures.

Estimating Coulomb Interactions U_n and J_{mn}

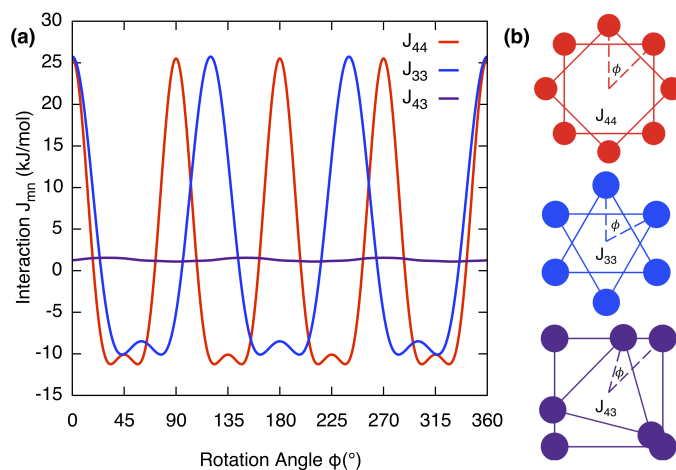


Fig. 5 (a) Inter-disc coulomb potentials J_{mn} as a function of rotation angle ϕ for rings in plane rotated around an axis perpendicular to their respective centres at the experimentally determined inter-disc separation of 3.8\AA . (b) Simplified rings of cations rotating about their respective centres, for the three separate configurations considered. Anions are not shown but included in the calculations, see Figure S2[†].

Coulomb interactions inside the supramolecular core, namely U_n and J_{mn} , are difficult to calculate since the exact arrangement is unknown. However this can be estimated by considering an

idealised symmetric ring of alternating cations and anions, see Figures 5b and S2[†]. This serves as an order of magnitude estimate, the intra-disc interactions U_4 and U_3 , were calculated to be -479289 (J/mol) and -479198 (J/mol) respectively. Inter-disc interactions were estimated by rotating these rings in plane around an axis perpendicular to their respective centres at the experimentally determined inter-disc separation of 3.8Å. The interaction parameter for like rings J_{nn} were always found to have an attractive minimum whereas unlike rings J_{mn} are always repulsive. This can be seen in Figure 5a, where the minima correspond to $J_{44} = -11241.2$ (J/mol) and $J_{33} = -10090.2$ (J/mol) at 45° or 60° respectively.

Solving the 1D Column & Introducing a Mean Field

To solve the model we draw analogy with the spin 1/2 Ising model⁴⁴, by writing the projection operator, $P_i^{(n)}$, in terms of $\sigma_i = \pm 1$.

$$P_i^{(4)} = \frac{1}{2}(1 + \sigma_i) \quad P_i^{(3)} = \frac{1}{2}(1 - \sigma_i) \quad (5)$$

The Hamiltonian takes a convenient form

$$\mathcal{H} = -K \sum_i \sigma_i \sigma_{i+1} - C(T) \sum_i \sigma_i + \text{const} \quad (6)$$

Here

$$K = \frac{1}{4}(2J_{43} - J_{44} - J_{33}) \quad (7)$$

$$C(T) = \frac{1}{2} \left((F_3(T) - F_4(T)) + (U_3 - U_4) + (J_{33} - J_{44}) \right) \quad (8)$$

This is then solved via the transfer matrix method⁴⁴. The expectation value of $\langle \sigma \rangle$ can be expressed exactly in terms of the parameters K and $C(T)$, where T_c occurs at $C(T) = 0$.

$$\langle \sigma \rangle = \frac{\sinh \beta C(T)}{\sqrt{\sinh^2 \beta C(T) + e^{-2\beta K}}} \quad \beta = \frac{1}{k_B T} \quad (9)$$

Only nearest neighbour interactions along a single column are considered above, but a mean field interaction, standing for long range (intra- and inter-columnar) interactions, is crucial to achieve long range ordering and a first order transition between phases. Therefore, two additional energy parameters, λ and μ , are introduced; the first disfavours mixing of unlike discs/columns and the second reduces impurities in the region $T < T_c$. This changes Equation 8 to Equation 10 and this means that the solution must be obtained numerically.

$$C'(T) = C(T) - \lambda \langle \sigma \rangle - \mu \langle \sigma \rangle^2 \quad (10)$$

Discussion

The free energy of the chains $F_n(T)$ is evaluated by examining their conformations on a diamond lattice in the confinement of the segment (1/3 or 1/4 of the disc) as described above. The intra-disc Coulomb interactions $U_3 - U_4$ were calculated assuming a near circular arrangement of alternating anions/cations in

the core of the disc, see Figures 5 and S2[†]. The interactions between neighboring cores that were obtained from the fitting, see Table 1, $J_{33} - J_{44}$ and K , were smaller than those calculated from the Coulomb interactions between the cores. Several important interactions were not included in the calculation: these include the interactions between the benzene rings and between the chains. The mean field interaction terms, $\lambda = 115$ J/mol and $\mu = 190$ J/mol, which are significantly smaller than the nearest neighbour interaction K , are additional fitting parameters. Note that K is equivalent to the χ parameter in the theory of polymer solutions and blends. The reason that such small additional terms are so important here is because even in their absence there are very long regions of order along the chains because $K/k_B T_c \sim 1.8$ which is greater than unity. Figure 6 depicts the effect of each of the above described interactions on the shape of the phase transition. Panel (i) shows how a supramolecular column might behave without interaction between its constituent discs: the free energy of the end chains $F_n(T)$ alone would prefer a mixed (43) phase with increasing preference for (3) at higher temperatures; and introducing the intra-disc interactions U_n stabilizes the (4) phase at lower temperatures. This clearly shows a competition between the entropy-driven end chains and energy-driven core interactions. Panel (ii) describes the behavior of the column with nearest neighbor interactions J_{mn} . In this case an ordered column in the (4) phase is stable over a considerable T -range and may then continuously transform to the (3) phase via the mixed (43) phase. Comparing (i) and (ii), it is clear that core-core interactions are responsible for the stable formation of columns. The effect of long range (intra- and inter-columnar) interactions are shown in (iii) and (iv): λ is responsible for the sharpness of the transition, and μ for the imbalance in tolerance to impurities in (4) and (3) phases. This allows us to produce the characteristic transition shape seen experimentally in Figure 2b.

Our results demonstrate that the observed transition is driven predominantly by the entropy of the end chains. In our quantitative fitting, the only explicitly temperature dependent term is the free energy of the chains. With increasing temperature the entropy of the end chains of the minidendrons increases due to the growing number of gauche defects, see Figure 4. This leads to the expulsion of minidendrons from the disc, which are now able to overcome the attractive energies holding them together.

The size of the inter-disc $J_{33} - J_{44}$ in comparison to the intra-disc $U_3 - U_4$ would suggest that discs of 4 minidendrons cannot exist without forming a column to stabilise their structure. Once a column is formed the discs are effectively locked into the column by the attraction between their head groups. By increasing temperature, the free energy of the end chains eventually allows for expulsion of a minidendron; when this occurs the entire column is destabilised leading to a sudden runaway expulsion of minidendrons down the column. This is true for an isolated column where K is the only parameter responsible for the continuity/discontinuity of the transition. Further increasing K would lead to a completely symmetric strongly first order transition effectively destroying the characteristic tail seen experimentally. The discontinuity and asymmetry in the transition must result from the attractive energy between the columns themselves.

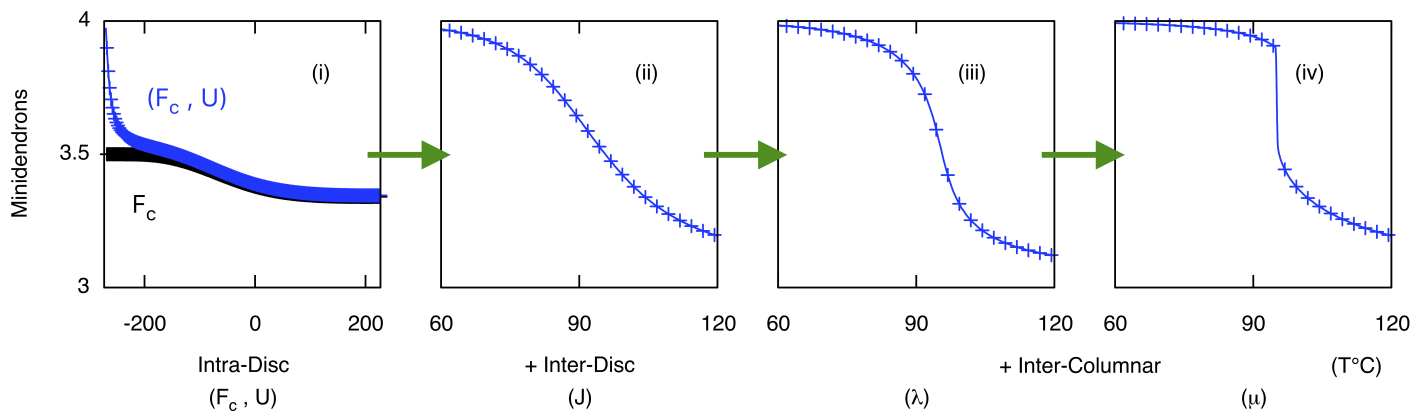


Fig. 6 Average number of molecules per disc as a function of temperature as different interactions are introduced, parameter values can be found in Table 1. (i) using core free energy F_c and intra-disc interactions U_n alone (ii) inter-disc interactions J_{mn} added, and (iii/iv) long range inter-columnar interaction parameters λ and μ included. Note the temperature range in (i) is significantly larger than (ii), (iii) and (iv).

Table 1 Calculated vs fitted parameters for the model fit shown in Figure 2, all values stated are in J/mol unless otherwise indicated and T_1 is indicated in Figure 4 at 227°C.

| | U_3 | U_4 | J_{33} | J_{44} | J_{43} | $U_3 - U_4$ | $J_{33} - J_{44}$ | K | $F_3(T_1) - F_4(T_1)$ | λ | μ |
|------------|---------|---------|----------|----------|----------|-------------|-------------------|------|-----------------------|-----------|-------|
| Calculated | -479289 | -479198 | -10090 | -11241 | 1096 | -91 | -1151 | 5881 | -2746 | - | - |
| Fitted | -479289 | -479198 | -10130 | -11985 | 0 | -91 | -1855 | 5529 | -2746 | 115 | 190 |

As we approach the critical point from low T , any supramolecular disc which transitions would break the long range order between columns, triggering this energetic transition to occur. The λ and μ terms are then absolutely necessary. Long range interactions are responsible for the discontinuity in the transition, as well as the temperature range over which the (4) phase remains stable.

A clear asymmetry is present in the transition which suggests the supramolecular columns in the (4) phase are able to tolerate the pressure due to the lateral expansion of the end chains with increasing temperature. The characteristic high-temperature tail would suggest that, once shedding has occurred, some (4) discs still exist due to the free space made available by the transition. However even these remaining discs are then gradually lost at higher temperatures. The resilience of the pure (4)-columns below the transition may be, at least partially, due to additional intra-columnar interactions that develop in (4)-columns, reflected in the appearance of a weak 7.4Å near-meridional diffraction feature (Figure 1c). While the main meridional diffraction at 3.7Å comes from the stacking of individual discs, the weak 7.4Å arc indicates pairing of adjacent discs. Most likely the successive discs are rotated in-plane by 45°, minimizing repulsion between alkyl chains and making the column a quadruple 8₁ helix (see Figure 5 and Coulomb energy calculations in SI[†]). It should be noted that neither the 3.7Å nor the 7.4Å reflect true long-range order. Upon the Col_h1-Col_h2 transition the 3.7Å peak shifts to 3.9Å indicating some tilting of the benzene rings away from the xy plane. At the same time the 7.4Å feature disappears, meaning that the extra intra-columnar order is lost in the mixed (43) columns.

In contrast to 12Na, 12Li maintains 3-dendron columns in the entire temperature range of the Col_h phase from 70°C to above 120°C. The smaller number of dendrons in 12Li discs is attributed to the tight-binding small Li⁺ ions drawing the dendron cores

closer to the column centre thereby effectively increasing the molecular taper compared to that of 12Na. We also note that the fibre pattern of the purely (3)-columns of 12Li (Figure 1d) again contains a clear 7.4Å arc, suggesting relatively high intra-columnar order; this time possibly of a triple 6₁ helical type (60° rotation between successive discs). Shrinkage of the purely (3)-columns of 12Li appears to be completely prevented, at least up to the temperature at which columns turn into spheres that form the cubic phase (Figure 2).

This strong resistance to shrinkage and the raising of T_c beyond the range of stability of the columnar phase is primarily due to a weaker intra-disc cohesion U_2 of the (2)-disc. In addition to the lower Coulomb energy of (2)-discs, the ample volume left empty by the removal of the third molecule and the resulting breaking of van der Waals bonds between alkyl chains must contribute significantly to raising the energy of the (2) phase. The extra conformational entropy achieved by turning 120° segments into 180° is clearly insufficient to offset the energy penalty at these moderate temperatures.

However it has been shown recently that addition of free alkane overcomes this obstacle and allows continuous thermal shrinkage of the (3)-columns in 12Li at moderate temperatures⁴². It was established, using labeled alkane and neutron scattering that, following dendron expulsion, the alkane collects preferentially in the resulting (2)-columns replacing the missing dendrons, effectively increasing U_2 by re-establishing the missing van der Waals bonds. Furthermore we noted the transition in 12Li starts continuous. Interestingly, the (3)-columns and the (2)-columns were found to occupy defined positions on a 2D superlattice with a three-column hexagonal unit cell. By analogy, it is expected that addition of alkane could turn the shrinkage of (4)-columns in 12Na from discontinuous to continuous.

Experimental Methods

The synthesis has been described previously^{10,11}. Powder SAXS experiments were conducted on beamline I22 of the Diamond synchrotron, and the fiber patterns on a Rigaku rotating anode source with multilayer mirrors and a MAR 345 image-plate detector. DSC was recorded on a Perkin-Elmer Pyris instrument at 5 K/min. Prior to the experiments the samples were vacuum dried for 24 hours and kept in sealed capillaries during the X-ray experiments.

Conclusions

We have reported the first example of a transition between two columnar phases of the same symmetry. To our knowledge this is also the first case of a transition based entirely on a change in the number of molecules in a self-assembled aggregate. We have described the transition quantitatively. The model is quasi one-dimensional because the largest interactions are along the columns and only small long range interactions are needed to cause the phase transition. The transition is driven by the end chains of the minidendrons that expand as the temperature is raised. This work is another demonstration of the principle of universality, which explains why similar behaviour is seen in disparate physical systems with the same dimensionality and number of degrees of freedom. In the original magnetic system the increase in temperature causes disorder along the spin chain, while in the system that is described here it also changes the sign of the ordering field.

Conflicts of interest

There are no conflicts to declare.

Acknowledgements

For help with synchrotron SAXS and fiber WAXS experiments we thank, respectively, Prof. Nick Terrill at I22, Diamond, and Dr. Patrick Baker at Sheffield University. Simulations were performed using the Sheffield Advanced Research Computer (ShARC) hosted by the University of Sheffield. Financial support is acknowledged from EPSRC (EP/K034308, EP/P002250), Leverhulme Trust (RPG-2012-804) and NSFC China (21274132).

References

- 1 H. J. Sun, S. Zhang and V. Percec, *Chem. Soc. Rev.*, 2015, **44**, 3900–3923.
- 2 B. Donnio, S. Buathong, I. Bury and D. Guillon, *Chem. Soc. Rev.*, 2007, **36**, 1495–1513.
- 3 C. Tschierske, *Angew. Chem. Int. Ed.*, 2013, **52**, 8828–8878.
- 4 T. Kato, N. Mizoshita and K. Kishimoto, *Angew. Chem. Int. Ed.*, 2006, **45**, 38–68.
- 5 V. Balagurusamy, G. Ungar, V. Percec and G. Johansson, *J. Am. Chem. Soc.*, 1997, **119**, 1539–1555.
- 6 D. J. Yeardley, G. Ungar, V. Percec, M. N. Holerca and G. Johansson, *J. Am. Chem. Soc.*, 2000, **122**, 1684–1689.
- 7 G. Ungar, Y. Liu, X. Zeng, V. Percec and W.-D. Cho, *Science*, 2003, **299**, 1208–1211.
- 8 X. Zeng, G. Ungar, Y. Liu, V. Percec, A. E. Dulcey and J. K. Hobbs, *Nature*, 2004, **428**, 157.
- 9 R. Zhang, X. Zeng and G. Ungar, *J. Phys.: Condens. Matter*, 2017, **29**, 414001.
- 10 G. Ungar, V. Percec, M. N. Holerca, G. Johansson and J. A. Heck, *Chem. Eur. J.*, 2000, **6**, 1258–1266.
- 11 V. Percec, M. N. Holerca, S. Uchida, W.-D. Cho, G. Ungar, Y. Lee and D. J. Yeardley, *Chem. Eur. J.*, 2002, **8**, 1106–1117.
- 12 M. A. Shcherbina, A. V. Bakirov, A. N. Yakunin, U. Beginn, L. Yan, M. Möller and S. N. Chvalun, *Soft Matter*, 2014, **10**, 1746–1757.
- 13 S. Hecht and J. M. Fréchet, *Angewandte Chemie International Edition*, 2001, **40**, 74–91.
- 14 F. Würthner, C. Thalacker, S. Diele and C. Tschierske, *Chem. Eur. J.*, 2001, **7**, 2245–2253.
- 15 Z. An, J. Yu, B. Domercq, S. C. Jones, S. Barlow, B. Kippelen and S. R. Marder, *J. Mater. Chem.*, 2009, **19**, 6688–6698.
- 16 G. Ungar, S. Batty, V. Percec, J. Heck and G. Johansson, *Adv. Funct. Mater.*, 1994, **4**, 303–313.
- 17 T. Ichikawa, M. Yoshio, A. Hamasaki, T. Mukai, H. Ohno and T. Kato, *J. Am. Chem. Soc.*, 2007, **129**, 10662–10663.
- 18 M. Peterca, V. Percec, A. E. Dulcey, S. Nummelin, S. Korey, M. Ilies and P. A. Heiney, *J. Am. Chem. Soc.*, 2006, **128**, 6713–6720.
- 19 C. S. Pecinovsky, E. S. Hatakeyama and D. L. Gin, *Adv. Funct. Mater.*, 2008, **20**, 174–178.
- 20 B. Soberats, M. Yoshio, T. Ichikawa, X. Zeng, H. Ohno, G. Ungar and T. Kato, *J. Am. Chem. Soc.*, 2015, **137**, 13212–13215.
- 21 G. Johansson, V. Percec, G. Ungar and D. Abramic, *J. Chem. Soc., Perkin Trans. 1*, 1994, 447–459.
- 22 A. Schultz, S. Laschat, A. Saipa, F. Gießelmann, M. Nimitz, J. L. Schulte, A. Baro and B. Miehl, *Adv. Funct. Mater.*, 2004, **14**, 163–168.
- 23 Y. Luo, N. Marets and T. Kato, *Chem. Sci.*, 2018, **9**, 608–616.
- 24 V. Percec, M. Glodde, T. Bera, Y. Miura, I. Shiyankovskaya, K. Singer, V. Balagurusamy, P. Heiney, I. Schnell and A. e. a. Rapp, *Nature*, 2002, **419**, 384.
- 25 T. T. Steckler, X. Zhang, J. Hwang, R. Honeyager, S. Ohira, X.-H. Zhang, A. Grant, S. Ellinger, S. A. Odom and D. e. a. Sweat, *J. Am. Chem. Soc.*, 2009, **131**, 2824–2826.
- 26 V. Percec, A. E. Dulcey, M. Peterca, P. Adelman, R. Samant, V. S. Balagurusamy and P. A. Heiney, *J. Am. Chem. Soc.*, 2007, **129**, 5992–6002.
- 27 B. Donnio, P. García-Vázquez, J.-L. Gallani, D. Guillon and E. Terazzi, *Adv. Funct. Mater.*, 2007, **19**, 3534–3539.
- 28 K. Kanie, M. Matsubara, X. Zeng, F. Liu, G. Ungar, H. Nakamura and A. Muramatsu, *J. Am. Chem. Soc.*, 2011, **134**, 808–811.
- 29 M. Matsubara, W. Stevenson, J. Yabuki, X. Zeng, H. Dong, K. Kojima, S. F. Chichibu, K. Tamada, A. Muramatsu and G. e. a. Ungar, *Chem.*, 2017, **2**, 860–876.
- 30 X. Feng, M. E. Tousley, M. G. Cowan, B. R. Wiesner, S. Nejadi, Y. Choo, R. D. Noble, M. Elimelech, D. L. Gin and C. O. Osuji, *ACS Nano*, 2014, **8**, 11977–11986.
- 31 Y. Li, S.-T. Lin and W. A. Goddard, *J. Am. Chem. Soc.*, 2004, **126**, 1872–1885.
- 32 P. Zihler and R. D. Kamien, *J. Phys. Chem. B*, 2001, **105**, 10147–10158.
- 33 P. de Gennes, *Liquid Crystals*, 1993.
- 34 S. John and T. Lubensky, *Phys. Rev. B*, 1986, **34**, 4815.
- 35 D. R. Nelson and B. Halperin, *Phys. Rev. B*, 1980, **21**, 5312.
- 36 J. Kosterlitz, *J. Phys. C*, 1973, **6**, 1181.
- 37 X. Zeng, R. Kieffer, B. Glettner, C. Nürnberg, F. Liu, K. Pelz, M. Prehm, U. Baumeister, H. Hahn, H. Lang et al., *Science*, 2011, **331**, 1302–1306.
- 38 S. George, C. Benthams, X. Zeng, G. Ungar and G. A. Gehring, *Phys. Rev. E*, 2017, **95**, 062126.
- 39 B. Mu, X. Hao, J. Chen, Q. Li, C. Zhang and D. Chen, *Polym. Chem.*, 2017, **8**, 3286–3293.
- 40 Y. K. Kwon, S. N. Chvalun, J. Blackwell, V. Percec and J. A. Heck, *Macromolecules*, 1995, **28**, 1552–1558.
- 41 X. Yao, L. Cseh, X. Zeng, M. Xue, Y. Liu and G. Ungar, *Nanoscale Horiz.*, 2017, **2**, 43–49.
- 42 M.-H. Yen, J. Chairapa, X. Zeng, Y. Liu, L. Cseh, G. H. Mehl and G. Ungar, *J. Am. Chem. Soc.*, 2016, **138**, 5757–5760.
- 43 P. J. Flory and M. Volkenstein, *Statistical mechanics of chain molecules*, 1969.
- 44 H. A. Kramers and G. H. Wannier, *Phys. Rev.*, 1941, **60**, 252.